https://doi.org/10.1016/j.tws.2019.106355

Performance of single-coped beam with slender web and quantification of local web buckling strength

Michael C.H. Yam[b,c], Ke Ke[a, b, *], Angus C.C. Lam[d] and Qingyang Zhao[a, b]

[a] *Hunan Provincial Key Laboratory for Damage Diagnosis of Engineering Structures, Hunan University, Changsha, China*

[b] *Department of Building and Real Estate, The Hong Kong Polytechnic University, Hong Kong, China*

[c] *Chinese National Engineering Research Centre for Steel Construction (Hong Kong Branch), The Hong Kong Polytechnic University, Hong Kong, China*

[d] *Department of Civil and Environmental Engineering, University of Macau, Macau, China*

Abstract: This paper reports a numerical study on the local web buckling strength and behaviour of single-coped beam with slender web (SCBSW). First, finite element (FE) models of SCBSW connections were developed, and the effectiveness of the modelling techniques was validated by the results of full-scale SCBSW connection tests conducted by the authors and those in the literature. Subsequently, an extensive parametric investigation covering a wide range of web slenderness ratio, cope geometries and rotational stiffness of the connection was conducted. A database of the FE results of 243 SCBSW models connected with a rotationally rigid support was developed. The analysis results show that all of the models were governed by local web buckling, and post-buckling behaviour of the SCBSW connections was confirmed. The interaction among the slender web, cope configurations and rotational stiffness of the connections on the structural behaviour and local web bucking capacity of SCBSW connections was characterised. A practical approach for evaluating the local web buckling strength of end-plate type SCBSW connecting with a rotationally rigid support was developed using the available FE results. The post-buckling behaviour and the interactive effect among the slender web and the other essential factors were considered in the proposed method. The proposed method produces reasonable predictions of the local web buckling strength of SCBSW connections with a rotationally rigid support comparing with those predicted by the FE results and the available test data, which may offer a basis for a full-fledged design guide for SCBSW.

Keywords: single-coped beam, slender web, local web buckling, post-buckling behaviour, finite element analysis, parametric study.

*Corresponding author. kerk.ke@outlook.com, keke@hnu.edu.cn

1. Introduction

To produce identical elevations for flanges at intersecting beam connections in a typical steel structure, the secondary beam ends are often coped (notched) to eliminate interference of the intersecting beams at the connections [1]. In engineering practice, either the top flange or both flanges at the beam end may need to be coped depending on the specific structural design details. Fig. 1 shows the schematics and a photo of typical coped beam connections. Although the cope (notch) configuration at the junction of the intersecting girders produces a neat connection, the flange(s) removal inevitably results in significant reduction of load carrying capacity of the connection compared with the uncoped counterpart.

Coped beam connections are susceptible to various local failures [1-4]. Local web buckling failure of coped beam connections as a common failure mode has attracted interests from the research community since it was characterised in the 1980s. Based on a detailed finite element (FE) parametric study, Cheng et al. [5, 6] examined the load carrying behaviour of coped beam connections with the compression flange removed, and they developed practical design recommendations for estimating the local web buckling capacity of single-coped beam connections using a plate buckling analogy. The adequacy of the design approach was confirmed by a full-scale test programme conducted by Cheng and Yura [5, 6], and the design approach was later included in the design manual of AISC [7] as guidelines for practitioners. Recognising that shear action may dominate the connection behaviour when the ratio of the cope length (c in Fig. 1) to the height of the coped web (h_0 in Fig. 1) is not significant, Yam et al. [8] proposed an alternative design model governed by a shear plate buckling analogy. Aalberg [9] carried out an experimental study on the load carrying behaviour of coped I-section beam connections with simply-supported boundary conditions at the coped ends, and the author also examined the effectiveness of existing design methodologies for designing single-coped beam connections. More test results were later reported by Aalberg [10] with the focus on aluminium coped beam connections, and it was confirmed that the shear-plate-based model developed by Yam et al. [8] produces satisfactory predictions of the local web buckling strength of the connections. In summary, the studies mentioned above on the local web buckling performance of single-coped beam connections generally emphasised hot-rolled I-section beams. In these scenarios, the web had a relatively smaller slenderness ratio, i.e. the ratio of the web height (h_w) to the web thickness (t_w) (Fig. 1), which was below 57.1.

It is common to use plate girders [11] for long span structures due to their higher moment resistance comparing to the counterparts with compact cross-sections of equivalent weight [12-14]. Since the web plate in a plate girder is usually slender, coping at the girder ends for intersecting beam connections would make the coped ends more susceptible to local web buckling. As mentioned, the current design methods for evaluating the local web buckling strength of coped beams are based on studies of hot-rolled members with relatively compact webs of low-to-intermediate web slenderness ratio. Therefore, these current design methods may not be suitable for evaluating the local web buckling strength of coped beams (girders) with slender web. To fill this research gap, the authors and colleagues initiated an investigation [15] aiming to examine the structural behaviour of SCBSW connections with the emphasis on the local web buckling performance. Based on an experimental programme including eleven (11) full-scale SCBSW connections with a rotationally rigid support [15], it was observed that the web slenderness ratio appreciably influences the load carrying behaviour of the connections, and this factor may further interact with the cope configuration (i.e. the coped length and the cope depth). In addition, it was found that the current design methods produced overly conservative estimates of local web buckling resistance of SCBSW connected to a rotationally rigid support.

In order to develop a suitable method for evaluating the local web buckling strength of coped beams with slender web, a numerical study was conducted. An extensive parametric analysis of 243 FE models of end-plate-type SCBSW connections covering a reasonable spectrum of influential parameters was performed. The main parameters included the web slenderness ratio, cope geometries, and the rotational stiffness of the connection. The effect of the initial geometric imperfection on the behaviour of SCBSW connections was also examined. A practical approach to predict the local web buckling strength of SCBSW connections was subsequently proposed.

2. Modelling techniques and verification

2.1. Test data pool

The available test results of SCBSW connections from two independent test programmes were used to verify the modelling techniques in the current work. In particular, test results from the experimental works conducted by the authors [15] and that of a specimen reported by Cheng et al. [5, 6] were used. The core information about the specimens in [15] is reproduced in Table 1. The experimental investigation included eleven (11) end-plate-type SCBSW connection specimens with non-compact I-sections, and the measured beam depth to web thickness ratio (D/t_w) of the test beams ranged from 102.9 to 157.1. The definition of the symbols is illustrated in Fig. 1. To facilitate reference, test codes were assigned to each specimen to reflect the web slenderness ratio and the cope geometry [15]. The initial capital letter ‘A’, ‘B’ and ‘C’ corresponds to specimens with the designed D/t_w ratio of 100, 125 and 150, respectively. The cope length is represented by the value after the capital letter, and the detail of the cope depth follows (i.e. the value after letter ‘dc’). In addition, one SCBSW connection specimen from Cheng’s work [5, 6], i.e. specimen coded as ‘PB26A’, was also examined in the numerical study. The information about this SCBSW connection is reproduced in **Appendix A** (Table A1), and more detail can be found in [5].

2.2. Modelling techniques

The finite element (FE) analysis package ABAQUS [16] was adopted to develop the FE models and simulate the responses of the twelve (12) SCBSW test connections mentioned above. The FE models of the test connections were discretised by four-node shell elements with reduced integration and a large strain formulation (i.e. the S4R elements). After a mesh sensitivity analysis, the general mesh size used was approximately 15 mm, and in the vicinity of the coped web area the element size was refined to about 5 mm. The material property of steel was replicated by utilising a combined kinematic material model governed by the von Mises yield criterion. In the material module, engineering stress versus engineering strain curves from the coupon tests were converted to true stress versus true strain responses for the FE model. In the models, the welds between the plate components, i.e. fillet welds between the flanges and the web and that connecting the end-plate and the web, were simulated by the 'merge' strategy in ABAQUS. Thus, the effect of the mechanical characteristics of the 'welding' was not included in the modelling. Nonetheless, this strategy was reasonable due to the fact that all the SCBSW connections were dominated by buckling failure, and hence the stress in the weld region generally stayed at a low level during the entire test. A typical FE model is shown in Fig. 2a. The boundary conditions were defined to simulate the constraints provided by the test rig. To eliminate the localised effect induced by the concentrated loads, the 'kinematic coupling' was adopted to constrain the translational and rotational degree-of-freedoms of nodes in the loading area and the support area, and the area (Fig. 2a) of the coupling region was identical to that of the loading plate and the supporting plate used in the test rig. The lateral movement constraint offered by the braces for preventing overall buckling of the test beams was also simulated in the FE models. Nonetheless, minor flexibility of the lateral bracing systems composed of steel angles and wood blocks (to minimise the effect of friction force) was neglected, and a fully laterally restrained boundary condition was assumed for the test beams at the bracing points (Fig. 2a) in the FE modelling.

The analysis followed a two-step framework by initiating an eigenvalue analysis as the first step, in which the fundamental elastic buckling mode of the SCBSW connections was captured. As an elastic analysis, both material nonlinearity and geometric nonlinearity was excluded from the first step. In the second step, a nonlinear static analysis procedure, i.e. the 'Riks' [16], was adopted to predict the nonlinear response of the models under monotonic loading, and the buckling shapes determined in the first step was introduced as the 'initial geometric imperfection'. It is worth mentioning that the fundamental buckling mode is of significant interest from the perspective of imperfection simulation, and it was utilised as the predefined initial geometric imperfection in the nonlinear analysis. A sensitivity analysis was performed to examine the influence of the amplitude of the initial geometric imperfection on the behaviour of the SCBSW connections. Four levels of initial geometric imperfection amplitude which were used in previous works [15, 17], i.e. 1%, 10%, 30% and 50% of t_w (t_w = web thickness), were considered in the analyses of each model to maintain consistency. The effect of the initial imperfections will be examined in detail in Section 2.3. In this step, both the material nonlinearity and the geometric nonlinearity were included.

2.3. Verification of the FE modelling

The reaction force of the connection (R) versus vertical deflection of the load point (δ) curves predicted by the FE analyses are correlated with the test data as shown in Fig. 3. In particular, the comparison between the FE responses and the test responses of the SCBSW connections studied by the authors [15] is presented in Fig. 3a and the comparison of specimen 'PB26A' from Cheng et al. [5, 6] is shown in Fig. 3b. In general, the reaction force versus vertical deflection curves predicted by FE models matched the test response well, and the equilibrium path of a SCBSW connection could be reasonably captured by the FE model. The analysis results based on various levels of initial geometric imperfection amplitudes show that the responses of the models with a less slender web are moderately sensitive to the amplitude of the initial geometric imperfections. However, the load-deflection curves of the models with a more slender web become less sensitive to the initial imperfection. In addition, increasing the coped length and the cope depth may aggravate this trend. These observations may be due to the fact that post-buckling mechanism is more evident for cases with a slender web and a larger cope, echoing findings from the pilot numerical study reported in [15]. According to the analysis results, it was further confirmed that utilising 10% of t_w as the assumed initial geometric imperfection amplitude produces a reasonable estimate of the ultimate strength for all the SCBSW connections in the literature, and the corresponding ultimate strengths of the connections predicted by the FE analyses, i.e. R_{FE}, are summarised in Table 1. Hence, this amplitude of initial geometric imperfection was adopted in the parametric studies. Typical buckling modes of the FE models compared well with those obtained from the test programme as shown in Fig. 4.

To further justify the adequacy of the FE model for quantifying the nonlinear response of the SCBSW connections, the reaction force versus lateral deflection curves of the FE models of the specimens [15] are presented in Fig. 5. The figure shows that the test reaction versus lateral deflection curves generally compare well with those of the FE models, except for specimens 'A300dc60' and 'A600dc60'. For these cases, the measured lateral deflection in the test increased with increasing applied load in the initial loading stage, however, the deflection was reversed and increased rapidly after buckling was triggered. This inconsistency might be induced by the difference between the actual initial geometric imperfection modes and the fundamental buckling mode which was consistently used in the numerical analysis. Nonetheless, the general trend of the reaction force versus lateral deflection curves of the SCBSW connections was characterised well by the FE models. Strain readings at the critical cross-sections for the SCBSW connections obtained by FE analyses and those extracted from the test database are generally correlated, as given in Fig. 6, where the amplitude of initial geometric imperfection was assumed as 10% of t_w. In particular, strain responses at 20%, 40% and 60% of the maximum load of the SCBSW connections are illustrated, and the ability of the FE models for characterising the behaviour of the SCBSW connections is seen.

3. Parametric investigation

3.1. Development of the parameter matrix

Based on the validated FE modelling techniques discussed in Section 2, an extensive parametric study was undertaken to examine the local web buckling performance of the SCBSW connections. The parametric study was commenced by analysing 243 models of end-plate-type SCBSW connections. Plate girders with various web slenderness ratios and cope dimensions were included in the study, and the parameter matrix is summarised in Table 2. The detailed information about the reference plate girders and the geometry of the corresponding SCBSW connections is shown in Appendix A (i.e. Table A2), which is also schematically shown in Fig. 2b. In particular, the beam depth (D) was varied from 600 mm to 900 mm, and the web thickness (t_w) was correspondingly set from 4 mm to 9 mm to produce a beam depth to web thickness ratio (D/t_w) between 100 and 150. The cope length (c) to beam depth ratio (c/D) ranging from 0.5 to 1.0 accompanied by a cope depth (d_c) to beam depth ratio (d_c/D) varied from 0.1 to 0.3 was included in the parameter matrix.

To maintain consistency, the lateral boundary condition was identical to those used in the model validation discussed in Section 2 (Fig. 2). The in-plane boundary condition used was consistent with those used in the validation study. To offer an in-depth understanding of the influences of connection rotational stiffness (*K*), the analyses were expanded to consider three end-plate thicknesses, i.e. 8 mm, 12 mm and 16 mm, and the details of the end-plate is shown in Fig. 1. Note that *K* is quantified by the slope of the linear stage of the moment-rotation response curve of the connection subjected to a hogging moment, and it can be readily obtained using an elastic analysis of the FE model. A summary of the parameters considered in the study is shown in Table 2.

In the analyses, grade S355 steel was used for all the models. The essential material properties of steel (i.e. elastic modulus, yield strength, and ultimate strength) for the nonlinear analysis were based on the nominal values documented in EC3 [11], and the ultimate strain (i.e. the strain at ultimate strength) for the S355 steel was assumed to be 15% [11, 17]. A magnitude of 10% of t_w for the fundamental buckling mode from an eigenvalue analysis was assumed as the initial geometric imperfection. To facilitate discussion, model designations were assigned to the FE database. Specifically, the model designation starts with the beam depth and web thickness (unit: mm) and is followed by the cope geometry (i.e. the cope length and the cope depth). The information about the thickness of the end-plate is shown at the end of the code. For example, the designation 'D600tw4c300dc60E8' stands for a SCBSW connection with beam depth (D) = 600 mm, web thickness (t_w) =4 mm, cope length (c) =300 mm, cope depth (d_c) = 60 mm, and end-plate thickness (t_e) = 8 mm.

3.2. Overview

The ultimate strength of the SCBSW models (R_{FE}) varied from 37.0 kN to 465.2 kN depending on the cross-section dimensions and cope details. The failure modes were confirmed by examining both responses curves and deformed patterns of FE results. Upon the ultimate load, it could be confirmed that all SCBSW connections were characterised by evident out-of-plane deformation of the coped web accompanied by a visible buckling line crossing the coped region. Concurrently, yielding of the coped section was not seen despite localised inelasticity detected in the coped corner. It is worth mentioning that the out-of-plane deformation of the coped web at the peak load generally increased with the D/t_w ratio, and the trend was more pronounced when a SCBSW connection model has a large cope size, i.e. a long and deep cope. Comparatively, for models with less slender webs and smaller cope sizes, the lateral movement of the coped web was relatively smaller when the ultimate strength was achieved, but an evident buckling line could be detected. This observation is consistent with that characterised in the test programme [15] and research findings from previous works on coped beam connections with a slender web [5, 6] or hot-rolled sections [8].

3.3. Load-deformation responses

Selected typical load versus in-plane deflection responses of the SCBSW connections are illustrated in Fig. 7. The dimensions of the presented FE models cover the beam depth to web thickness ratio (D/t_w) ranging from 100 to 150 (Fig. 7a). To demonstrate the interaction between a slender web and the cope geometry, representative load versus deflection responses of models with the cope depth to beam depth ratio (d_c/D) varying from 0.1 to 0.3 and the cope length to beam depth ratio (c/D) ranging from 0.5 to 1.0 are presented in the Fig. 7b and Fig. 7c. For clarity, the point characterising the ultimate strength is marked by a circle in the response curves. It can be seen from Fig. 7a that for models with the D/t_w ratio ranging from 100 to 150, the ultimate load increases with decreasing D/t_w ratio (increasing web thickness). In general, the load-deflection curves show typical linear behaviour in the early loading stage, whereas the characteristics of the nonlinear stage change with varied combination of the D/t_w ratio and the cope geometry. In particular, it can be seen that for models with a smaller cope length and cope depth, e.g. model D600tw4c300dc60E8, a sudden drop is characterised for the response curves and rapid deterioration of the connection strength can be observed in the post-ultimate stage. With increasing c/D ratio, the resistance deterioration in the post-ultimate stage is less evident. For the models with a larger cope length (e.g. model D600tw4c600dc60E8 with c/D = 1.0), a stable nonlinear stage is observed in the response curves with continued increase in applied load due to the post-buckling strength of the SCBSW connection as shown in Fig. 7. Moreover, the deformation range of the ascending branch generally increases with increasing D/t_w ratio.

Furthermore, it can be observed from Fig. 7b that the cope depth also interacts with the slender web component and the cope length, influencing the characteristics of the response curves of SCBSW connections. For example, comparing the response curves of model D600tw4c300dc60E8 with that of D600tw4c300dc180E8 as shown in Fig. 7b, it is seen that the characteristics of the load-deflection curves are quite different. The ascending branch of the load-deflection curve in the nonlinear stage is observed for specimen D600tw4c300dc180E8 which has the largest d_c/D ratio of 0.3. For cases with longer cope (e.g. comparing D600tw4c300dc60E8 and D600tw4c600dc60E8), a gradual unloading behaviour of the connections in the post-buckling stage is evident as illustrated in Fig. 7c.

3.4. Post-buckling strength of the SCBSW connection

In order to clearly illustrate the post-buckling strength of the SCBSW connection, the ultimate strength of the 243 SCBSW models by FE analysis (R_{FE}) is plotted against the corresponding elastic buckling strength (R_{EG}), as shown in Fig. 8. It is worth noting that R_{EG} was extracted from the eigenvalue analysis results using the static linear perturbation analysis module in ABAQUS [16]. It can be observed that the data points tend to cluster above the forty-five degree diagonal line with increasing D/t_w ratio, which is demonstrated by a separate local view shown in the figure. Thus, the contribution of a slender web to promoting the post-buckling behaviour of a SCBSW is further confirmed. It should be noted that Fig. 8 indicates that R_{FE} is lower than R_{EG} in some cases, which generally correspond to models with a less slender web or a smaller cope (either in length or in depth). In these cases, the post-buckling behaviour may not be fully developed due to insignificant membrane action of the coped region, and the presence of slight initial imperfection could result in reduction of the connection strength. This observation was also captured and discussed in the previous experimental work [15], and is echoed by the FE results discussed in Section 2.

3.5. Effects of parameters

3.5.1 General

Since similar observations were obtained for models with various beam depths, only typical FE predictions of ultimate strength of the SCBSW models with the beam depth of 600 mm are shown in Fig. 9. In particular, the ultimate strengths of the SCBSW connections predicted by the FE analyses were normalised by the connection reaction force causing yielding of the coped section ($R_y = M_y/c$, where M_y is the yield moment of the coped section, i.e. the T-section). The normalised resistance (R_n) is plotted against the studied parameters, i.e. the D/t_w ratio, the c/D ratio, the d_c/D ratio and the rotational stiffness of the connection (K, unit: 10^3 kNm/rad) as shown in Fig. 9 to demonstrate the effects of slender web, cope geometry and rotational restraint provided by the end-plate connection on the local web buckling strength of the SCBSW connections.

3.5.2 Effects of web slenderness ratio

As shown in Fig. 9a, the normalised connection resistance decreased with increasing D/t_w ratio. This observation was expected due to the fact that an increasing D/t_w ratio produced a more slender web, and the SCBSW connections were more susceptible to local web buckling. In this context, the ultimate strength of a SCBSW connection with a very slender web might be much lower than the corresponding yield strength. In addition, the rate of reduction of the normalised resistance generally decreased with increasing D/t_w ratio. This could be attributed to the mobilisation of post-buckling behaviour of the SCBSW connections, which is in line with the findings drawn from the experimental programme of SCBSW connections and a preliminarily numerical study [15]. A comprehensive study exploring a practical method quantifying the post-buckling resistance of the SCBSW connections will be addressed in later sections of this work.

3.5.3 Effects of cope geometry

The influence of the cope length to beam depth ratio (*c/D*) on the normalised resistance is illustrated in Fig. 9b. It should be noted that an increasing *c/D* ratio produced by an increasing cope length consistently compromised R_y. Nonetheless, the ultimate strength of the connection also decreased with an increasing *c/D* ratio. Due to the interactive effect mentioned above, the normalised resistance varied inconsistently with increasing *c/D* ratio. It is interesting and important to note that for models with a shallow cope, R_n generally decreased with an increasing *c/D* ratio, whereas this tendency was reversed in case of a deeper cope. For instance, in case of D/t_w =100 and d_c/D = 0.1, R_n was decreased by 9% with the c/D ratio increased from 0.5 to 1.0. In contrast, a correspondingly increasing R_n by 10% was recorded in case of D/t_w =100 and d_c/D = 0.2. In addition, the positive correlation between R_n and the c/D ratio was characterised in cases of a more slender web according to results in case of D/t_w =150 and d_c/D = 0.2, as R_n increased by 19% with c/D ratio increasing from 0.5 to 1.0. The effects of the d_c/D ratio on the normalised resistance were also inconsistent, as illustrated in Fig. 9c. In particular, in cases of a less slender web and a short cope (i.e. D/t_w =100 and c/D = 0.5), R_n generally decreased with increasing of the d_c/D ratio, whereas this tendency could be varied with increasing web slenderness and cope length. For instance, R_n of the FE models with D/t_w =100 and c/D = 0.7 decreased by 4% when the d_c/D ratio was increased from 0.1 to 0.2, whereas R_n increased by 9% with further increase of the d_c/D ratio to 0.3. In the scenario with a more slender web and a longer cope (i.e. D/t_w =150 and c/D = 1.0), R_n consistently increased with the d_c/D ratio. In general, a slender web with a deep cope or a long cope further reduces the constraint to the coped web plate offered by the top flange at the cope corner. Hence, the development of membrane action of the coped region may be easily triggered. As a result, the post-buckling resisting mechanism would be mobilised more readily, activating a positive correlation between R_n and the c/D ratio or the d_c/D ratio. These observations were in line with the findings from the test programme and the pilot FE study [15].

3.5.4 Effect of rotational restraint provided by the end-plate connection

Due to the presence of the rotational restraint of the connection, hogging moment can be induced in the vicinity of the cope, and hence reduces the compressive action in the coped web. To examine the influence of the rotational restraint provided by the end-plate connection, the normalised resistance (R_n) is plotted against the rotational stiffness of the connection (K) as shown in Fig. 9d. The models with D/t_w =150 are presented in the figure since the results of the other models show similar trend. Based on the rotational stiffness of the connection determined from the FE results (0. 11×10^3 kNm/rad <K< 0.57×10^3 kNm/rad), the end-plate connections of the 243 models were all classified as nominally pinned joints according to EC3 [11]. Nevertheless, the effect of rotational stiffness of the connection on the normalised resistance of the SCBSW models is shown in Fig. 9d. As can be seen from the figure, the normalised resistance increased almost linearly with the rotational stiffness. Since the yield strength (R_y) was constant with varied rotational stiffness of the end-plate, the increasing R_n confirmed the contribution of the rotational restraint on the local web buckling strength of a SCBSW connection.

To demonstrate the effect of the rotational stiffness of the end restraint, the moment distributions of typical FE models at the ultimate load were extracted using ‘Free Body Cut’ in ABAQUS [16], as shown in Fig. 9e. It can be confirmed that the hogging moment at the face of the end-plate increased with end-plate thickness, and the inflection point of a SCBSW connection was correspondingly more distant from the end plate. In this context, the compression action of the coped web with a more rigid connection could be mitigated, enhancing the local web buckling strength of a SCBSW connection.

4. Design considerations

4.1. Evaluation of existing design methods

The ultimate strengths of the SCBSW models predicted by the FE analyses are correlated with the design predictions by Cheng's and Yam's methods, as shown in Fig. 10. The detailed information about these design models is reproduced in **Appendix B** for clarity. Specifically, the local web buckling strengths of the connections predicted by Cheng's method (R_{Cheng}) are plotted against the FE predictions as shown in Fig. 10a, and the computed local web buckling strengths by Yam's method (R_{Yam}) are correlated with the FE results as illustrated in Fig. 10b. The direct comparison between the FE predictions and those by the current design equations along with the 20% discrepancy line is also shown in the figure. In general, the data clustered below the 20% discrepancy line, demonstrating the conservative nature of both Cheng's method and Yam's method in cases of SCBSW connections with a strong rotational restraint. In Fig. 10, a separate enlarged view is used to illustrate the models with the ultimate strength lower than 200 kN, which generally correspond to cases with a higher web slenderness ratio. According to the comparison between the data points and the 50% discrepancy line, it is observed that the design predictions by the existing methods are more conservative with increasing web slenderness ratio. In summary, Cheng's method produces a FE-to-predicted ratio ranging from 1.00 to 3.40 for the 243 SCBSW connection models, with a mean value of 1.83 and a corresponding coefficient of variation (CoV) of 0.27. Comparatively, Yam's method results in a FE-to-predicted ratio varying from 1.02 to 3.08. The mean FE-to-predicted ratio is 1.61 with a corresponding CoV of 0.24. The conservative predictions by both Cheng's method and Yam's method may be due to the fact that the test and numerical analysis results used to develop the design methods were based on coped beam specimens with compact webs of smaller web slenderness ratio. In addition, the post-buckling strength and behaviour of the coped web and the effect of the rotational stiffness of the end-restraint on enhancing the local web buckling strength of a SCBSW connection with rotationally rigid support have not been quantified in current design methods. Therefore, a practical computation method which could be used to estimate the post-buckling strength and the contribution of the end-restraint of a SCBSW connection with a rotationally rigid support may be in need to shed more insightful lights on the load carrying behaviour of the connection.

4.2. Framework and formulation of the method

In light of the above, although both Cheng's method and Yam's method are generally safe for estimating the local web buckling strength of a SCBSW, neglecting the post-buckling resisting mechanism and the contribution of rotational restraint to the connections could produce overly conservative predictions of the connection strength. To offer a comprehension of the load carrying behaviour and post-buckling resisting mechanism of a SCBSW connection with an end-plate restraint, the principal stress distribution including the maximum compressive stress ($\sigma_{\min}$) and the maximum tensile stress ($\sigma_{\max}$) of a representative model (i.e. D600tw4c300dc60E8) at the ultimate load are shown in Fig. 11. As expected, a tension field action is evident as illustrated by the maximum tensile stress distribution along the inclined buckling line after the connection progressed to the post-buckling stage. Comparatively, a non-uniform maximum compressive stress distribution across the path near the inclined tension field (i.e. X2 in Fig. 11) can be characterised, and a pronounced increase of compressive stress near the boundary of the web is observed. In general, these observations are in line with the stress state of a thin shear plate exhibiting evident post-buckling resistance [18], and are also echoed by the research finding that a single-coped beam with a practical cope (c/h_0 < 1.5) is dominated by shear buckling failure [8]. It should be re-emphasised that these findings are limited to coped beams connected to a rotationally rigid support.

Therefore, the shear-plate-based analogy proposed by Yam et al. [8] was used as the basis to develop a modified framework for quantifying the local web buckling strength of a SCBSW in the current work. Employing the shear plate based buckling model in [8], the critical shear stress of a single coped beam connection is reproduced as:

$$\tau_{\mathrm{cr}} = k_{\mathrm{s}} \frac{\pi^2 E}{12\left(1-\nu^2\right)}\left(\frac{t_w}{h_0}\right)^2 \tag{1}$$

where k_s = shear buckling coefficient; E = elastic modulus; ν = Poisson's ratio and other symbols are defined in Fig. 1, i.e. t_w = web thickness and h_0 = height of the coped web (i.e. the T section). Although Yam et al. [8] proposed an empirical equation for evaluating k_s, as reproduced in **Appendix B**, the design equation was developed based on a FE database of single-coped beam connections with relatively more compact webs of lower slenderness ratio. To account for the effect of a slender web and the interaction among the slender web with the cope configuration, k_s is re-evaluated using the FE database including 243 models of SCBSW connections in the current study. Based on the elastic buckling strength of SCBSW connections (R_{EG}) extracted from the FE results (i.e. by eigenvalue analyses), k_s is given by

$$k_s = \frac{R_{EG}}{t_w\left(D-d_c\right)} \cdot \frac{12\left(1-\nu^2\right)}{\pi^2 E}\left(\frac{h_0}{t_w}\right)^2 \tag{2}$$

Utilising the shear plate model proposed by Yam et al. [8], k_s can be quantified by the following equations, given by

$$k_s = a\left(\frac{h_0}{c}\right)^b \tag{3}$$

$$a = a_1\frac{d_c}{D} + a_2 \tag{4}$$

$$b = a_3\left(\frac{d_c}{D}\right)^2 + a_4\frac{d_c}{D} + a_5 \tag{5}$$

where a_1, a_2, a_3, a_4 and a_5 and are coefficients which may be determined based on a curve fitting procedure. Utilising the FE database of SCBSW models in the current study, the coefficients in Yam's model are re-evaluated, and hence it is recommended that a_1 = -2.70, a_2 = 1.73, a_3 = 5.50, a_4 = -4.35, and a_5 =2.00. The convergence criterion of the curve fitting procedure was governed by the least square principle. It is re-emphasised that the regressed coefficients may be limited to cases falling in the parameter matrix (i.e. SCBSW connections with rotational rigidity, $100 \leqslant D/t_w \leqslant 150$, $0.5 \leqslant c/D \leqslant 1.0$, $0.1 \leqslant d_c/D \leqslant 0.3$). Thus, the elastic buckling strength of a SCBSW connection can be determined by substituting Eqs. (1), (3), (4) and (5) into the following:

$$R_{cr} = \tau_{cr}(D - d_c)t_w \tag{6}$$

In addition, a modification factor (W) accounting for the effect of web slenderness ratio and cope geometries on enhancing the post-buckling resistance of a SCBSW connection is proposed. The following expression for W is proposed:

$$W = \left(c_1 \frac{D}{100t_w} + c_2\right)\left(\frac{h_0}{c}\right) + \left(c_3 \frac{D}{100t_w} + c_4\right) \tag{7}$$

where coefficients c_1, c_2, c_3 and c_4 were determined based on curve fitting of the results from the FE database examined in the current study, and are given as follows:

$$c_1 = 6.60\left(\frac{c}{D}\right)^2 - 8.72\left(\frac{c}{D}\right) + 1.47 \tag{8}$$

$$c_2 = -4.33\left(\frac{c}{D}\right)^2 + 3.70\left(\frac{c}{D}\right) + 0.14 \tag{9}$$

$$c_3 = -3.00\left(\frac{c}{D}\right)^2 + 2.50\left(\frac{c}{D}\right) + 1.91 \tag{10}$$

$$c_4 = -0.61\left(\frac{c}{D}\right)^2 + 4.40\left(\frac{c}{D}\right) - 3.08 \tag{11}$$

Moreover, a modification factor, Q_v, is proposed to account for the influences of the rotational restraint of the end-plate connection on the local web buckling behaviour of the SCBSW connection. Utilising a regression analysis, the following expression for Q_v is developed:

$$Q_v=\left\{\left(-4.95\frac{d_e}{100t_e}+2.03\right)\frac{d_e}{h_0}+\left(1.44\frac{d_e}{100t_e}+0.45\right)\right\}\left(0.37\frac{D}{100t_w}+0.55\right) \quad (12)$$

where d_e = end-plate depth and t_e = end-plate thickness. Therefore, building on the design framework developed by Yam et al. [8] with modifications mentioned above, the design strength of a SCBSW (R_{Mo}) is given by

$$R_{Mo}=WQ_vR_{cr} \quad (13)$$

Again, it should be kept in mind that the calibrated coefficients in this section may be limited to cases within the parametric spectrum, as summarised in Table 2.

4.3. Validation of the proposed design method and comments

To demonstrate the improved accuracy of the proposed method for estimating the elastic buckling strength of SCBSW connections, the design predictions by Yam's equation [8], i.e. R_{Yam}, and the proposed modification, i.e. R_{cr} determined by Eqs. (1), (3), (4), (5) and (6), is compared with the elastic buckling strength of SCBSW connections (i.e. R_{EG}) in a normalised form, as shown in Fig. 12a. In particular, the design predictions were normalised by the shear yield strength of the connection, i.e. $R_{vy} = f_{vy}h_0t_w$, where f_{vy} is the shear yield strength of material. These normalised strengths (i.e. R_{Yam}/R_{vy} and R_{cr}/R_{vy}) are plotted against the normalised slenderness ratio, i.e. $\lambda_w = (f_{vy}/\tau_{FE})^{0.5}$, where τ_{FE} is the critical shear stress determined by FE analysis ($\tau_{FE} = R_{FE}/h_0t_w$), as shown in Fig. 12a. Therefore, it can be seen that the modified equations developed in this study provide better predictions of the elastic buckling strength of SCBSW connections comparing to those predicted by Yam's method, as the predictions in a normalised form (i.e. R_{cr}/R_{vy}) by the modified method are closer to FE predictions.

Utilising the proposed method, the design predictions (i.e. R_{Mo}) of 243 SCBSW models are correlated with FE predictions (i.e. R_{FE}), as shown in Fig. 12b. As can be seen, the data points are clustered close to the forty-five-degree diagonal line, and the discrepancies for most models are generally within 20%. In general, a mean FE-to-predicted ratio of 1.00 is achieved, and the corresponding CoV is 0.04. Thus, the proposed modified design approach offers a more accurate prediction of local web buckling strength of the SCBSW connections with rotational stiffness compared with the existing methods (i.e. Cheng's method and Yam's method). To further justify the validity of the proposed computation method, the ultimate strengths of the test SCBSW connections conducted by the authors [15] are compared with the design predictions (R_{Mo}), as shown in Table 1. The predictions by Cheng's method and Yam's method are also compared with the corresponding test results as shown in the table. In general, the proposed design equation is able to provide satisfactory predictions of the test results when comparing to those based on either Cheng's or Yam's methods. The test-to-predicted ratio based on the proposed design equation ranges from 0.91 to 1.20 with a mean of 1.05 and a corresponding COV of 0.08. Thus, the enhanced accuracy of the proposed method for quantifying the local web buckling strength of SCBSW connections with a rotationally rigid support falling in the parametric study ($100 \leq D/t_w \leq 150$) is demonstrated.

It also should be re-emphasised that the method is limited to a SCBSW connection with a rotationally rigid support (e.g. a main girder with effective torsional restraint, column flange, and in the case where coped beams are connected to both sides of a main girder). Note that the influence of flexible supporting boundary conditions on the strength and behaviour of a double coped beam has also been confirmed in a previous study [19].

5. Design example

To demonstrate the use of the proposed method, an illustrative example of an end-plate SCBSW connection is given in this section. The section of the beam is 600 × 150 × 5 × 8, and the thickness of the end-plate is 8mm. The coped length (c) equals 480 mm and cope depth (d_c) equals 150 mm. Thus, the cope length to beam depth ratio is equal to 0.80 and the cope depth to beam depth ratio is equal to 0.25. The yield stress of the beam is 355 MPa, and the elastic modulus (E) is 210 GPa. The Poisson's ratio (ν) is 0.3. The configuration of the SCBSW connection is shown in Fig. 13. Although this cope geometry is not examined in the parametric study, it is within the parameter matrix of this work.

Employing the design equations proposed in this paper, the shear buckling coefficient k_s is calculated as

$$k_s = a\left(\frac{h_0}{c}\right)^b = 1.06 \times 0.94^{1.26} = 0.98$$

where

$$a = 1.73 - 2.70\frac{d_c}{D} = 1.73 - 2.70 \times 0.25 = 1.06$$

$$b = 5.50\left(\frac{d_c}{D}\right)^2 - 4.35\frac{d_c}{D} + 2.00 = 5.50 \times 0.25^2 - 4.35 \times 0.25 + 2.00 = 1.26$$

Then the critical shear stress is calculated by the following equation:

$$\tau_{cr} = k_s \frac{\pi^2 E}{12\left(1-\nu^2\right)}\left(\frac{t_w}{h_0}\right)^2 = 0.98 \times \frac{3.14^2 \times 210000}{12 \times \left(1-0.3^2\right)} \times \left(\frac{5}{450}\right)^2 = 22.94 \text{ MPa}$$

The critical reaction R_{cr} is calculated as:

$$R_{cr} = \tau_{cr} t_w h_0 = 22.94 \times 5 \times 450 = 51.62 \text{ kN}$$

The modification factor W is calculated by the following equations:

$$c_1 = 6.60\left(\frac{c}{D}\right)^2 - 8.72\left(\frac{c}{D}\right) + 1.47 = 6.60 \times 0.8^2 - 8.72 \times 0.8 + 1.47 = -1.28$$

$$c_2 = -4.33\left(\frac{c}{D}\right)^2 + 3.70\left(\frac{c}{D}\right) + 0.14 = -4.33 \times 0.8^2 + 3.70 \times 0.8 + 0.14 = 0.33$$

$$c_3 = -3.00\left(\frac{c}{D}\right)^2 + 2.50\left(\frac{c}{D}\right) + 1.91 = -3.00 \times 0.8^2 + 2.50 \times 0.8 + 1.91 = 1.99$$

$$c_4 = -0.61\left(\frac{c}{D}\right)^2 + 4.40\left(\frac{c}{D}\right) - 3.08 = -0.61 \times 0.8^2 + 4.40 \times 0.8 - 3.08 = 0.05$$

$$W = \left(c_1 \frac{D}{100t_w} + c_2\right)\left(\frac{h_0}{c}\right) + \left(c_3 \frac{D}{100t_w} + c_4\right) = \left(-1.28\frac{600}{100 \times 5} + 0.33\right)\left(\frac{450}{480}\right) + \left(1.99\frac{600}{100 \times 5} + 0.05\right) = 1.30$$

The modification factor Q_v is calculated as follows:

$$\begin{aligned} Q_v &= \left\{\left(-4.95\frac{d_e}{100t_e} + 2.03\right)\frac{d_e}{h_0} + \left(1.44\frac{d_e}{100t_e} + 0.45\right)\right\}\left(0.37\frac{D}{100t_w} + 0.55\right) \\ &= \left\{\left(-4.95\frac{250}{100 \times 8} + 2.03\right)\frac{250}{450} + \left(1.44\frac{250}{100 \times 8} + 0.45\right)\right\}\left(0.37\frac{600}{100 \times 5} + 0.55\right) = 1.07 \end{aligned}$$

Therefore, the predicted strength of the SCBSW connection by the approach proposed in this study is determined by:

$$R_{\mathrm{Mo}}=WQ_{\mathrm{v}}R_{\mathrm{cr}}=1.30\times1.07\times51.61=71.80\text{ kN}$$

A FE model of the SCBSW was also developed using the verified modelling techniques, and the local web buckling strength by FE prediction is 71.49 kN, which is just 0.4 % less than the result from the suggested recommendation. In contrast, Cheng's method [5, 6] and Yam' method [8] produced a design prediction of 39.5 kN and 45.2 kN, respectively.

6. Conclusions

This paper discusses the local web buckling performance of single-coped beam with slender web (SCBSW) connections and contributes to a practical approach for predicting the local web buckling strength. A finite element (FE) model to capture the nonlinear structural behaviour of SCBSW connections subjected to monotonic loading was developed. The adequacy of the developed FE models was validated by the results of eleven full-scale tests conducted by the authors and one from other researchers available in the literature. The sensitivity of the nonlinear load-deflection response of SCBSW connections to the initial geometric imperfections was evaluated using the available test database, and it was confirmed that the sensitivity of the load-deflection curve of a SCBSW connection to the initial imperfection is reduced with increasing web slenderness ratio and cope sizes (either in length or depth).

Based on the validated FE modelling techniques, an extensive parametric investigation of SCBSW connections covering a spectrum of web slenderness ratio, beam depth, cope geometries and rotational stiffness of the connection was initiated. The findings from the parametric study show that all of the models of SCBSW connections were governed by local web buckling failure. Post-buckling resistance mechanism was observed for the models of SCBSW connections, which is more evident when increasing the web slenderness ratio, the cope length and the cope depth. Moreover, the load carrying capacity of SCBSW connections also increases with increasing rotational stiffness of the connection.

To offer a practical tool for estimating the local web buckling strength of SCBSW connections with a rotationally rigid support, a computation approach using the plate shear buckling analogy was developed based on the FE database in the current work. The computation approach also includes the influence of the slender web, the beam depth, the cope geometry and the rotational restraint of the connection on the structural behaviour of SCBSW connections. It was observed that the proposed method produced satisfactory estimates of the local web buckling strength of SCBSW connections, which may offer a basis for developing a full-fledged design guide for SCBSW connections.

Acknowledgements

This research is funded by a grant from the Research Grants Council of the Hong Kong Special Administrative Region, China (project no. PolyU 152189/15E). Partial funding support by a grant from the Hong Kong Polytechnic University (project no. G-YBU9) is also gratefully acknowledged.

Appendix A

The information about a SCBSW connection examined by Cheng [5, 6] is reproduced in Table A1 for clarity.

The detailed information about 27 basic FE models used in the parametric study is given in Table A2. For each basic model, three levels of end-plate thickness (i.e. 8 mm, 12 mm and 16mm) and three *c*/*D* ratios (i.e. *c*/*D* = 0.5, 0.7 and 1.0) were further considered. Thus, a FE database of 27 × 3 × 3 = 243 models was formed. The definitions of the symbols are illustrated in Fig. 1.

Appendix B

For clarity, the design equations for estimating the local web buckling strength of single-coped beam connections are reproduced in Appendix B. In Cheng's method [5, 6], a triangular stress distribution pattern was assumed with the maximum stress at the top of the cope and zero at the bottom, and the critical stress (σ_{cr}) is expressed by

$$\sigma_{cr} = f \frac{k\pi^2 E}{12(1-\nu^2)} \left(\frac{t_w}{h_0}\right)^2 \qquad \text{(B1)}$$

where f = proposed modification factor and k = buckling coefficient of the panel. The other symbols in Eq. A1 are identical to those defined in Eq. (1). The k factor was further correlated with the aspect ratio of the coped region, i.e. the h_0/c ratio, reproduced as

$$\begin{cases} k = 2.2(\frac{h_0}{c})^{1.65} & \frac{c}{h_0} \le 1 \\ k = 2.2(\frac{h_0}{c}) & \frac{c}{h_0} > 1 \end{cases} \tag{B2}$$

The modification factor f was obtained based on simple curve-fitting, and the expressions are given by

$$\begin{cases} f = \frac{2c}{D} & \frac{c}{D} \le 1 \\ f = 1 + \frac{c}{D} & \frac{c}{D} > 1 \end{cases} \tag{B3}$$

Thus, the local web buckling capacity predicted by Cheng's method can be obtained by $R_{\mathrm{Cheng}} = \sigma_{\mathrm{cr}} Z/c$, where Z is the elastic section modulus.

In the design model proposed by Yam et al. [8], it was assumed that the local web buckling failure is dominated by shear buckling of the coped region, and the critical shear stress is reproduced by

$$\tau_{\mathrm{cr}} = k_{\mathrm{s}} \frac{\pi^2 E}{12(1-\nu^2)} (\frac{t_{\mathrm{w}}}{h_0})^2 \tag{B4}$$

Based on an FE database developed by Yam et al. [8], an empirical equation of the shear buckling coefficient (k_{s}) was proposed using a nonlinear regression analysis, as given by

$$k_{\mathrm{s}} = a(\frac{h_0}{c})^b \tag{B5}$$

$$a=1.38-1.79\frac{d_c}{D} \quad \text{(B6)}$$

$$b=3.64\left(\frac{d_c}{D}\right)^2-3.36\frac{d_c}{D}+1.55 \quad \text{(B7)}$$

Therefore, the local web buckling strength of a single-coped beam connection predicted by Yam's method can be obtained by $R_{Yam} = \tau_{cr}t_w h_0$.

References

[1] Yam MCH, Fang C, Lam ACC, Cheng JJR. Local failures of coped steel beams - A state-of-the-art review. J Constr Steel Res 2014; 102: 217-232.

[2] Cheng JJR. Design of steel beams with end copes. J Constr Steel Res 1993; 25(1-2): 3-22.

[3] Yam MCH, Cheng JJR. Fatigue strength of coped steel beams. J Struct Eng 1990; 116(9):2447-2463.

[4] Topkaya C. Finite element modeling of block shear failure in coped steel beams. J Constr Steel Res 2007; 63(4):544-553.

[5] Cheng JJR, Yura JA, Johnson CP. Design and behavior of coped beams. University of Texas at Austin. 1984.

[6] Cheng JJR and Yura JA. Local web buckling of coped beams. J Struct Eng 1986; 112(10): 2314-2331.

[7] American Institute of Steel Construction. Steel construction manual 15th edition, Chicago, Illinois, 2017.

[8] Yam MCH, Lam ACC, Iu VP, Cheng JJR. Local web buckling strength of coped steel I beams. J Struct Eng 2003; 129(1): 3-11.

[9] Aalberg A. Experimental and numerical parametric study on the capacity of

coped beam ends. J Constr Steel Res 2015; 113: 146-155.

[10] Aalberg A. Design of aluminium beam ends with flange copes. Thin-Walled Struct 2015; 94: 593-602.

[11] CEN. Eurocode 3: design of steel structures - part 1-1: general rules and rules for buildings. European Committee for Standardization, Brussels, Belgium; 2005.

[12] Chen Y, Cheng X, Nethercot DA. An overview study on cross-section classification of steel H-sections. J Constr Steel Res 2013, 80: 386-393.

[13] Cheng X, Chen Y, Nethercot DA. Experimental study on H-shaped steel beam-columns with large width-thickness ratios under cyclic bending about weak-axis. Eng Struct 2013; 49(2):264-274.

[14] Cheng X, Chen Y, Niu L, Nethercot DA. Experimental study on H-section steel beam-columns under cyclic biaxial bending considering the effect of local buckling. Eng Struct 2018; 174:826-839.

[15] Ke K, Yam MCH, Lam ACC, Chung KF. Local web buckling of single-coped beam connections with slender web. J Constr Steel Res 2018; 150: 543-555.

[16] ABAQUS Analysis User's Manual. ABAQUS Standard, Version 6.12; 2012.

[17] Yam MCH, Fang C, Lam ACC. Local web buckling mechanism and practical design of double-coped beam connections. Eng Struct 2016; 125: 54-69.

[18] Glassman JD, Moreyra Garlock ME. A compression model for ultimate postbuckling shear strength. Thin-Walled Struct 2016; 102:258-272.

[19] Johnston GG. Strength and behaviour of double-coped steel beams under combined loads. MSc thesis, Department of Civil and Environmental Engineering, University of Alberta, Candada, 2015.

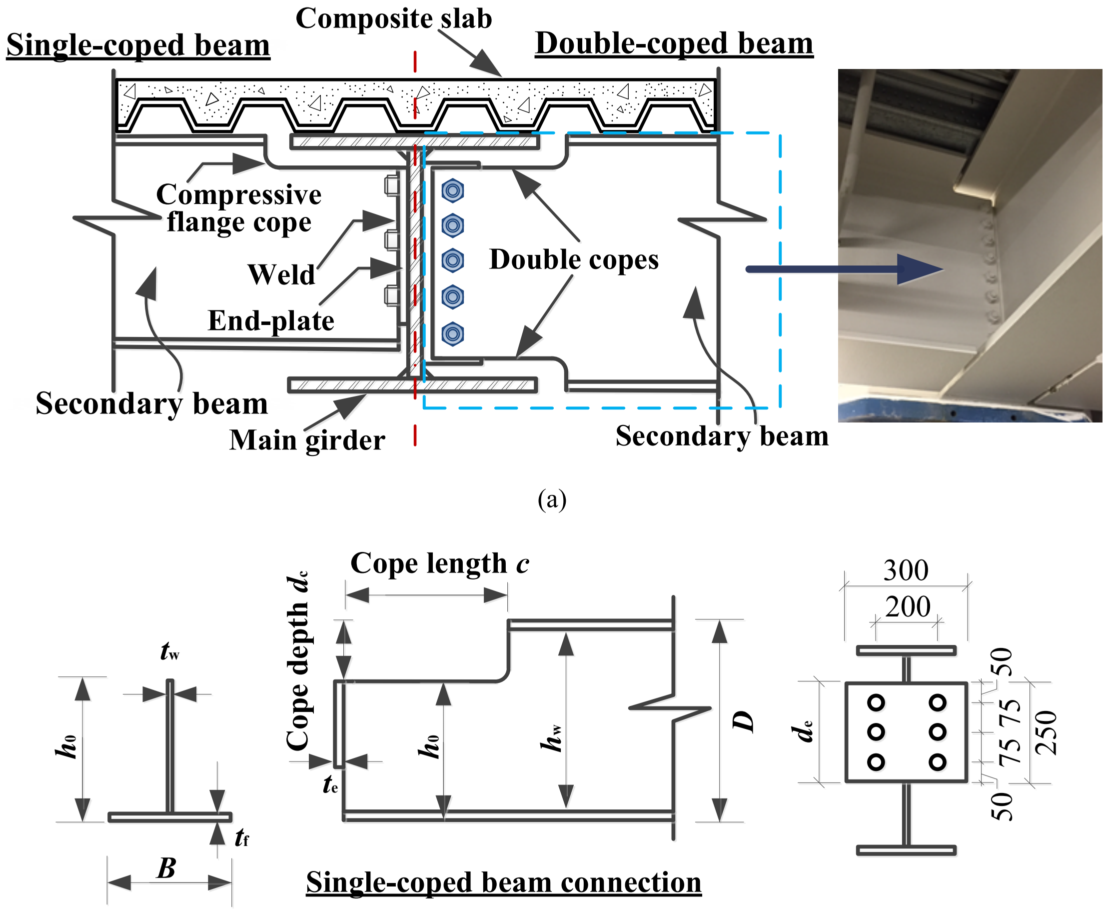

(a)

(b)

Fig. 1 Coped beam connections and key symbols: (a) cope beam connection and (b) symbols and end-plate detail.

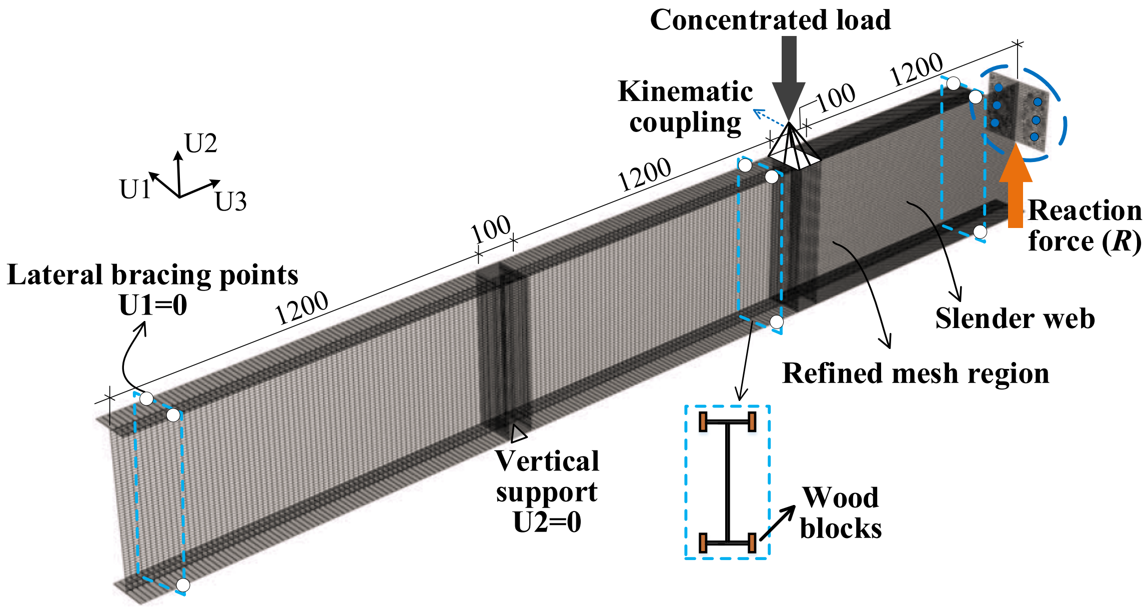

(a)

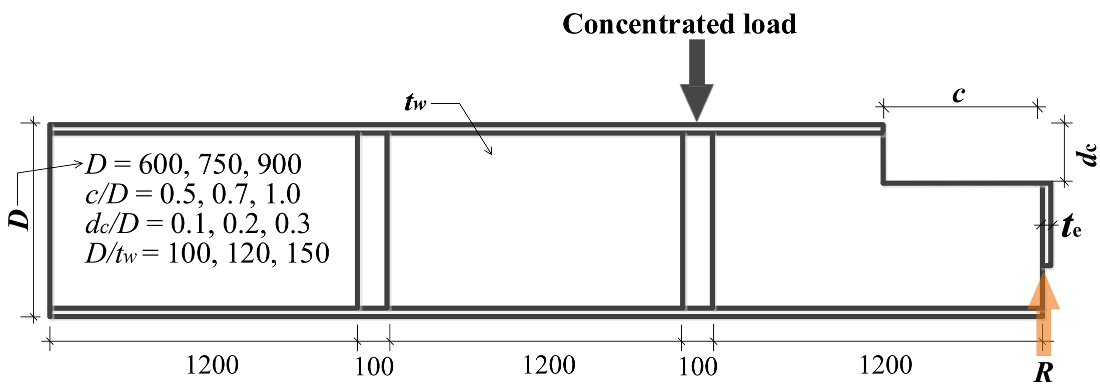

(b)

Fig. 2 Overview of finite element (FE) model: (a) modelling techniques and (b) Schematic illustration of FE models for the parametric study.

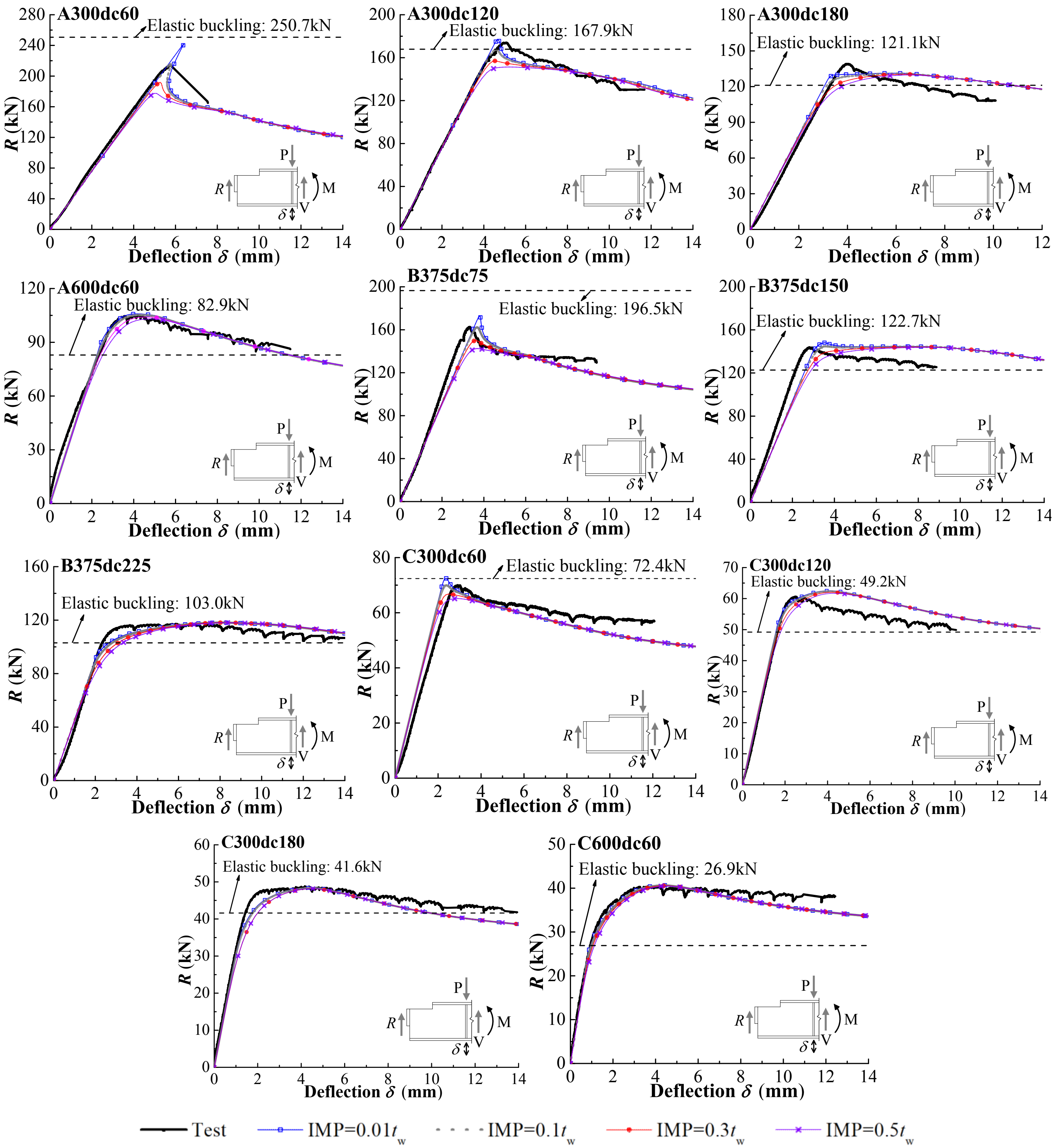
A300dc60
Elastic buckling: 250.7kN
A300dc120
Elastic buckling: 167.9kN
A300dc180
Elastic buckling: 121.1kN
A600dc60
Elastic buckling: 82.9kN
B375dc75
Elastic buckling: 196.5kN
B375dc150
Elastic buckling: 122.7kN
B375dc225
Elastic buckling: 103.0kN
C300dc60
Elastic buckling: 72.4kN
C300dc120
Elastic buckling: 49.2kN
C300dc180
Elastic buckling: 41.6kN
C600dc60
Elastic buckling: 26.9kN
R (kN)
Deflection δ (mm)
P
R
M
V
δ
Test
IMP=0.01t_w
IMP=0.1t_w
IMP=0.3t_w
IMP=0.5t_w

(a)

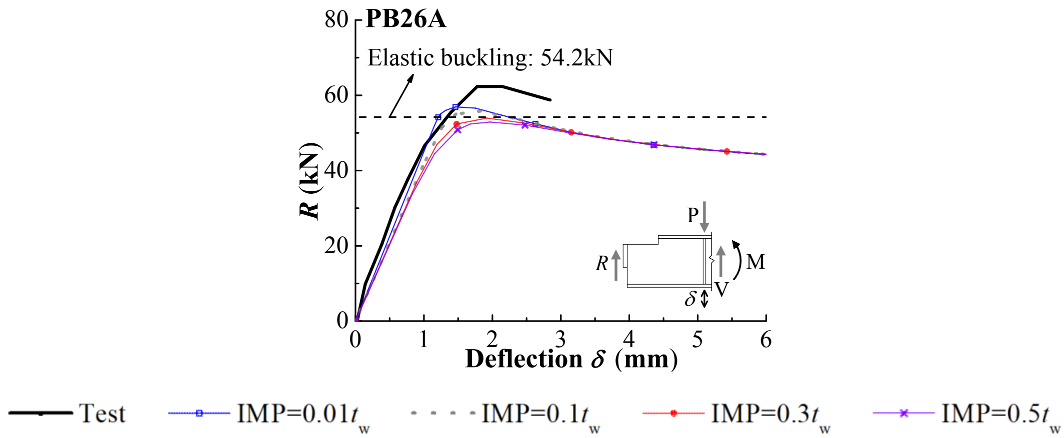

(b)

Fig. 3 Comparison of test responses and FE predictions: (a) SCBSW connections examined by the authors [15] and (b) SCBSW connections in Cheng's work [5, 6].

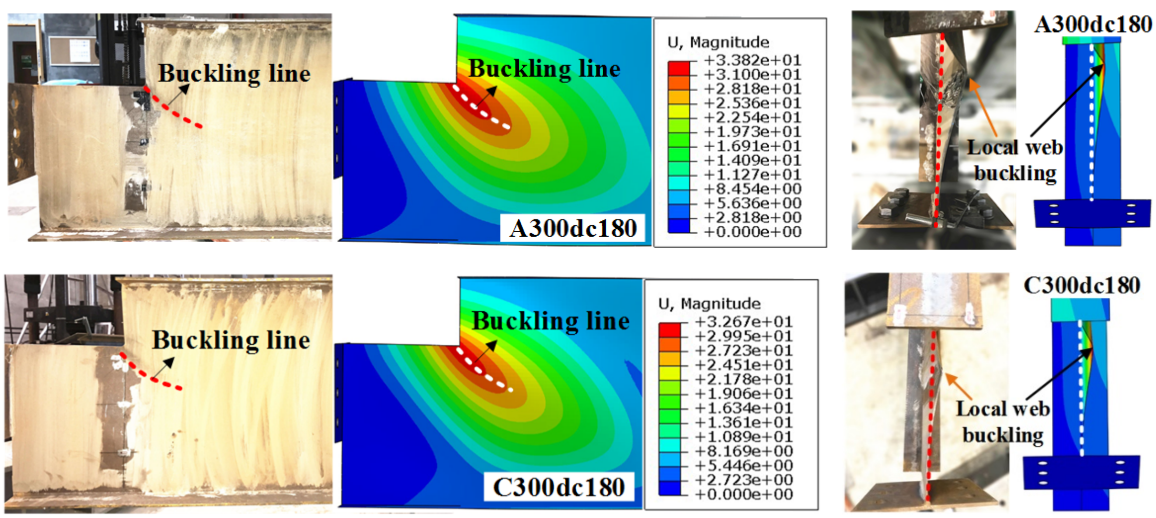

Fig. 4 Comparison of buckling modes between test results and FE simulations.

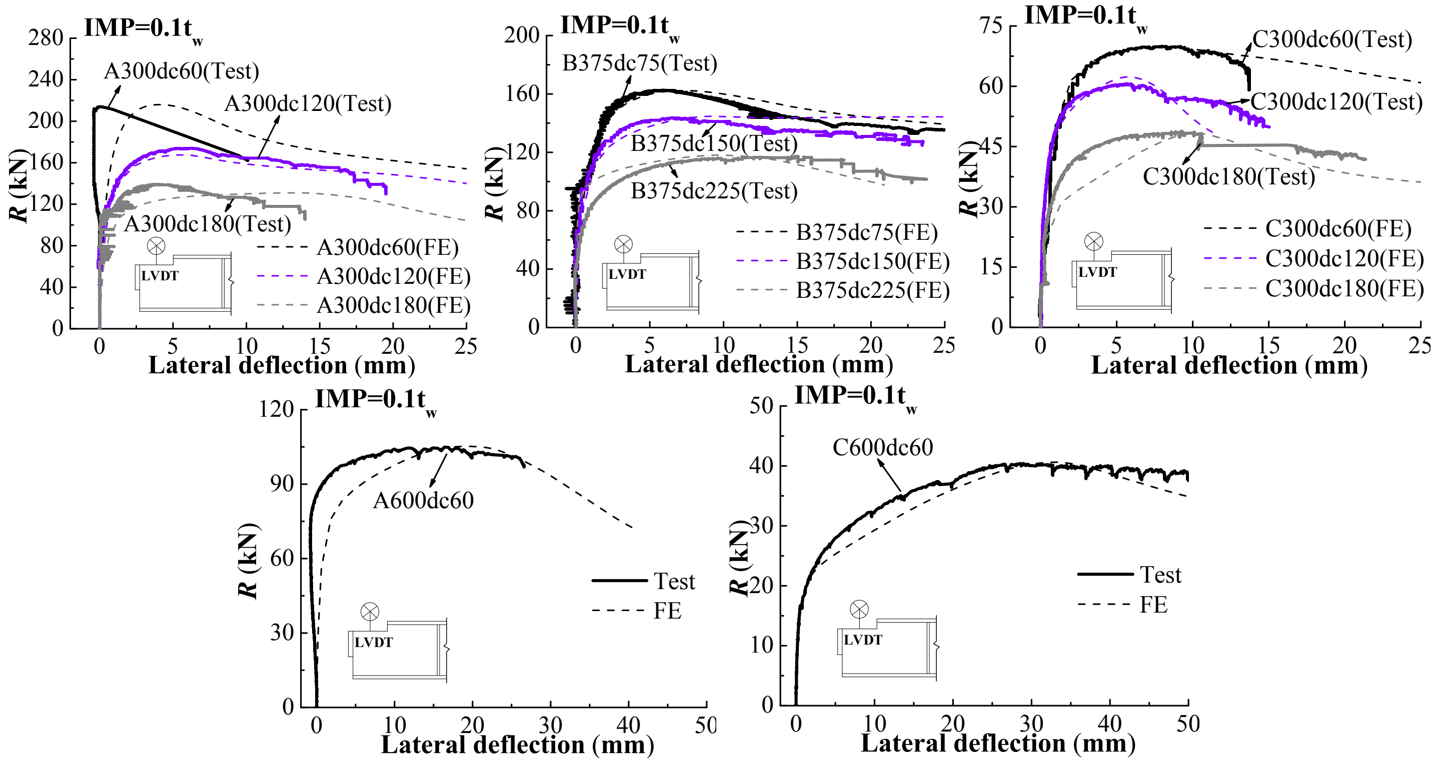

Fig. 5 Comparisons of connection reaction force versus lateral deflection responses.

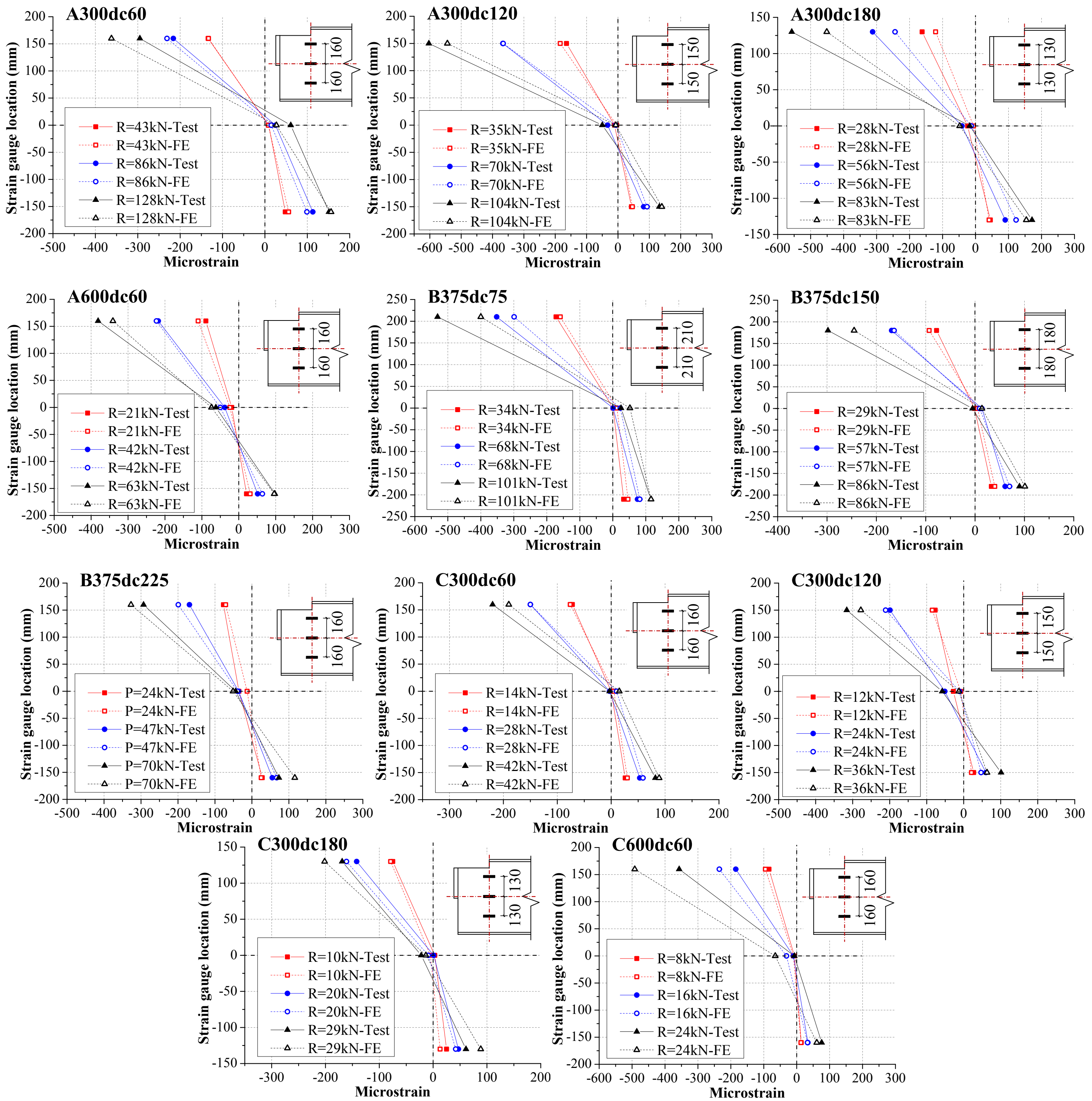

Fig. 6 Comparisons of strain gauge readings of the SCBSW connections.

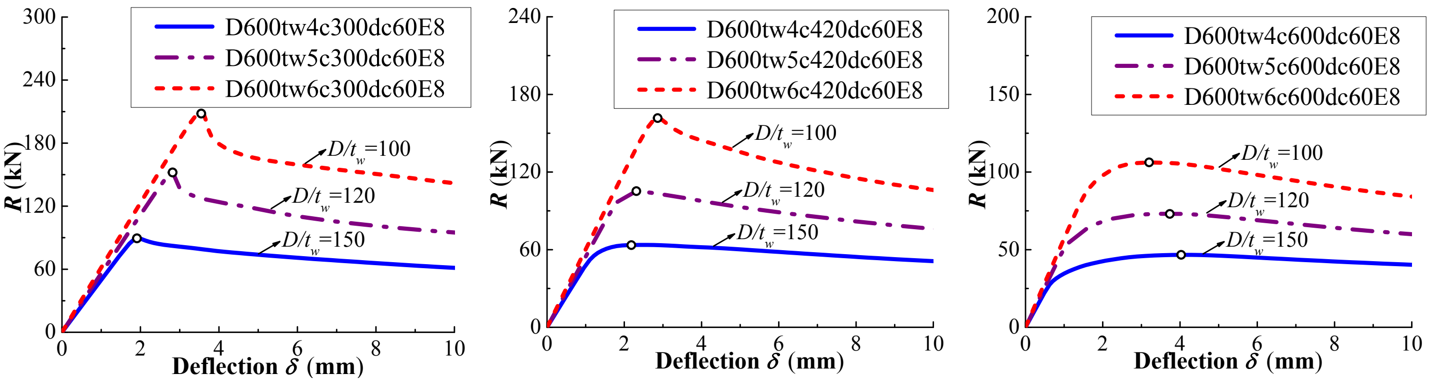

(a)

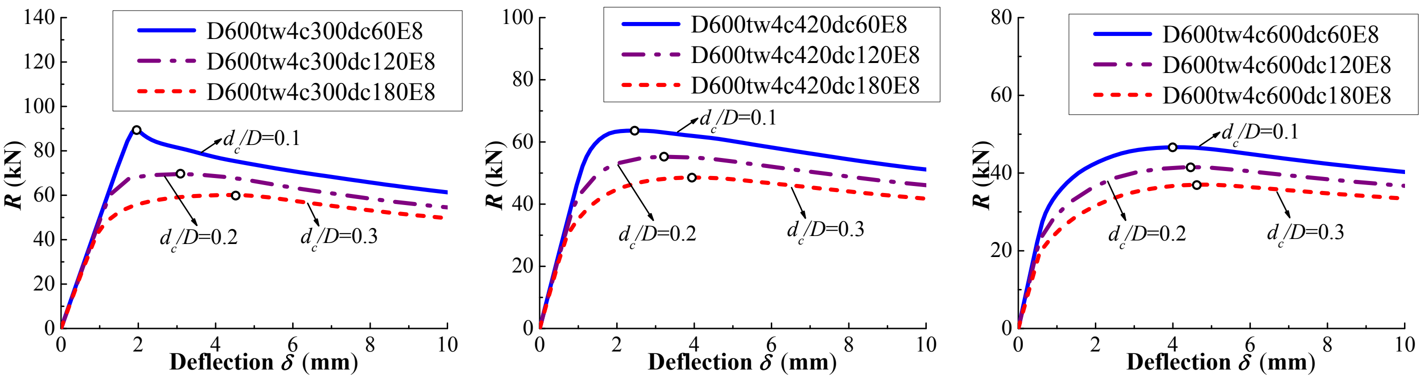

(b)

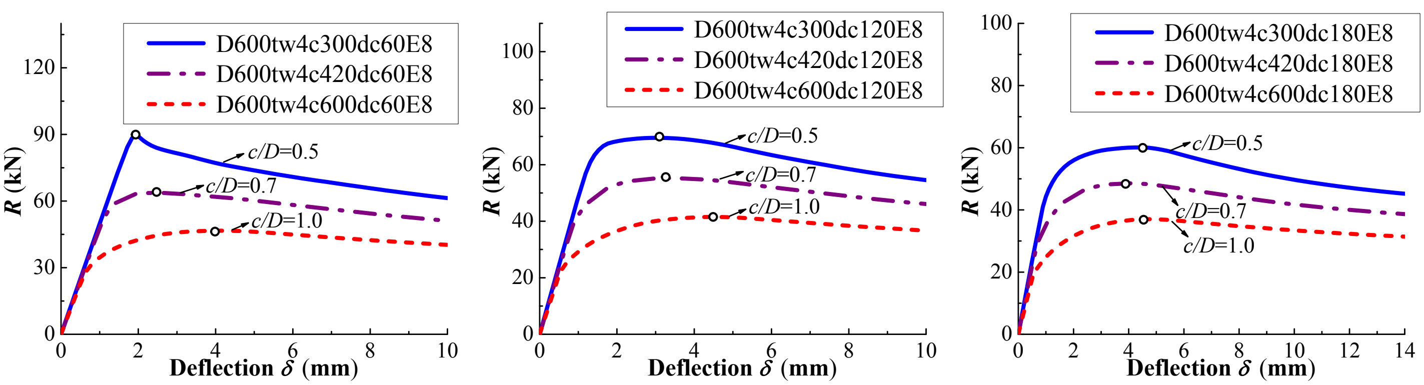

(c)

Fig. 7 Selected connection reaction force versus in-plane deflection responses (D= 600 mm): (a) D/t_w =100~150 (b) d_c/D =0.1~0.3 and (c) c/D =0.5~1.0

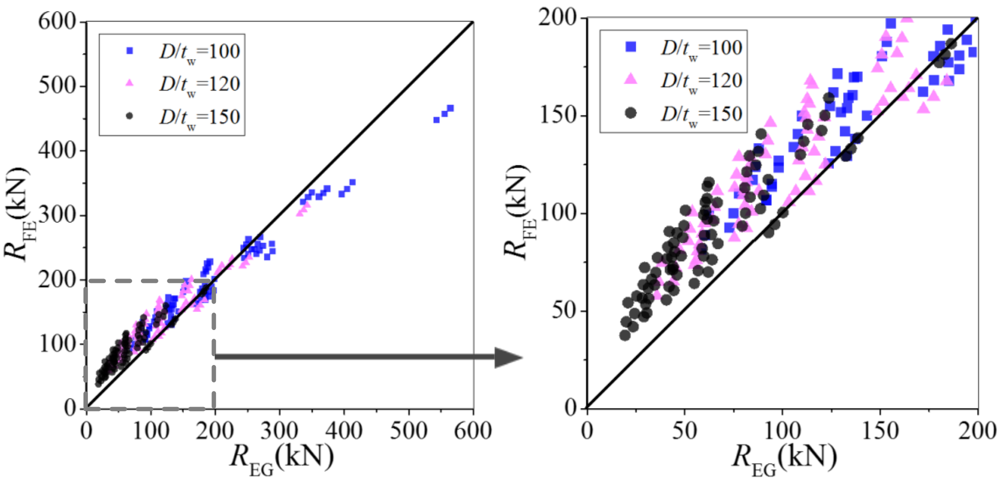

Fig. 8 Comparison between elastic buckling strength and FE results.

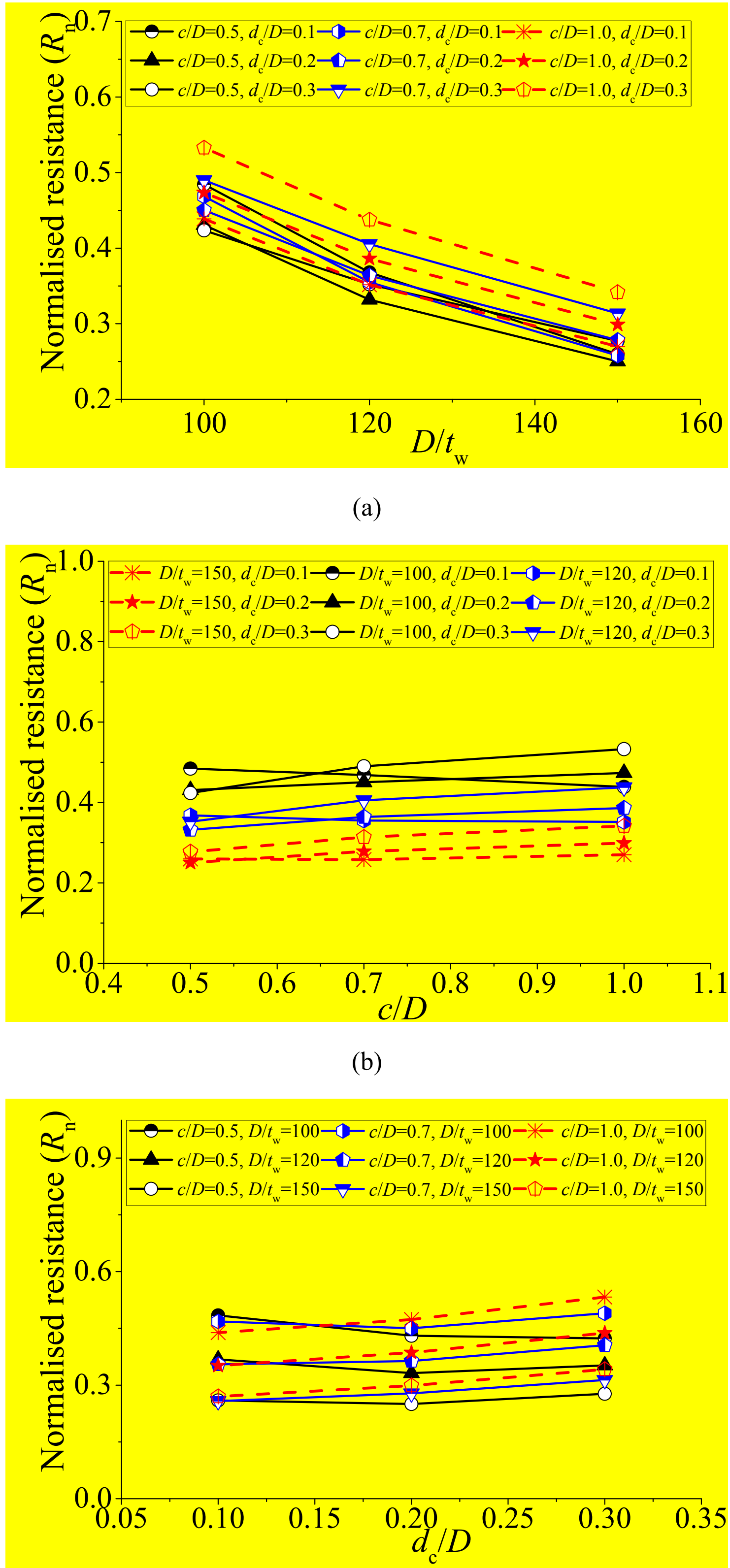

Normalised resistance (R_n)
D/t_w
c/D=0.5, d_c/D=0.1
c/D=0.5, d_c/D=0.2
c/D=0.5, d_c/D=0.3
c/D=0.7, d_c/D=0.1
c/D=0.7, d_c/D=0.2
c/D=0.7, d_c/D=0.3
c/D=1.0, d_c/D=0.1
c/D=1.0, d_c/D=0.2
c/D=1.0, d_c/D=0.3

(a)

Normalised resistance (R_n)
c/D
D/t_w=150, d_c/D=0.1
D/t_w=150, d_c/D=0.2
D/t_w=150, d_c/D=0.3
D/t_w=100, d_c/D=0.1
D/t_w=100, d_c/D=0.2
D/t_w=100, d_c/D=0.3
D/t_w=120, d_c/D=0.1
D/t_w=120, d_c/D=0.2
D/t_w=120, d_c/D=0.3

(b)

Normalised resistance (R_n)
d_c/D
c/D=0.5, D/t_w=100
c/D=0.5, D/t_w=120
c/D=0.5, D/t_w=150
c/D=0.7, D/t_w=100
c/D=0.7, D/t_w=120
c/D=0.7, D/t_w=150
c/D=1.0, D/t_w=100
c/D=1.0, D/t_w=120
c/D=1.0, D/t_w=150

(c)

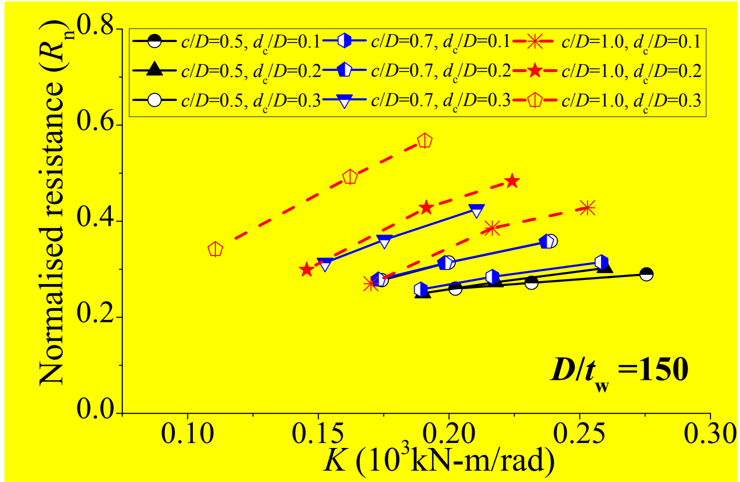

(d)

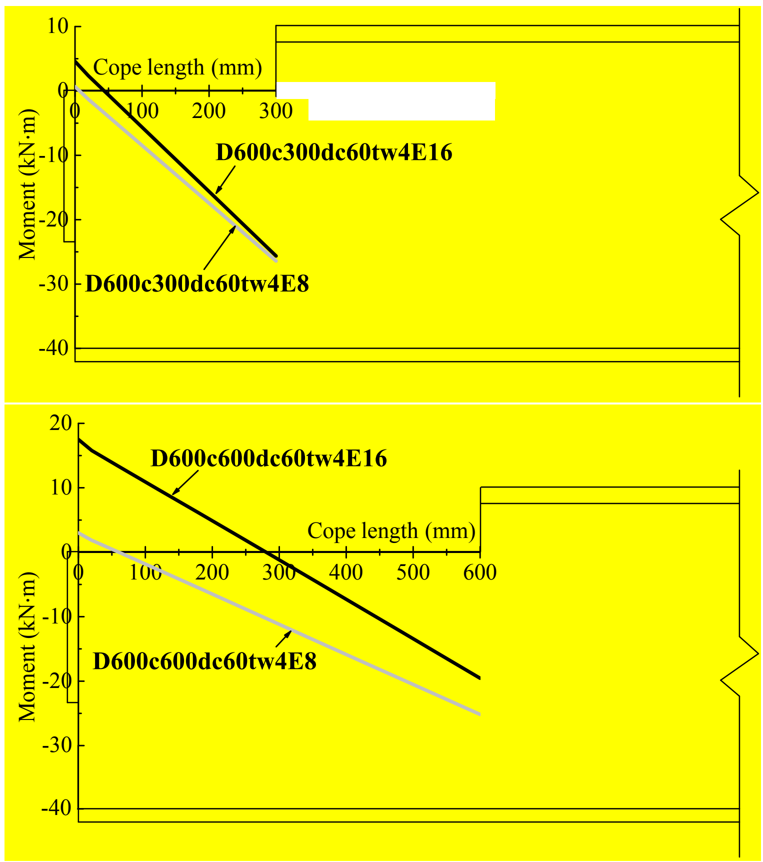

(e)

Fig. 9 Effect of parameters on the resistance of SCBSW connections: (a) effect of the D/t_w ratio (b) effect of the c/D ratio (c) effect of the d_c/D ratio (d) effect of the rotational stiffness of the connection and (e) moment distribution in the cope for typical models with varied end-plate thickness.

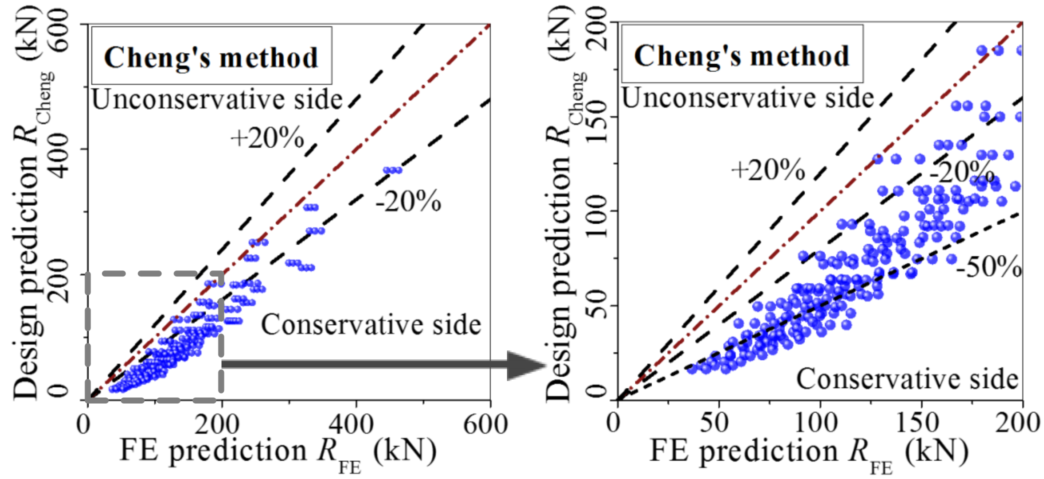

(a)

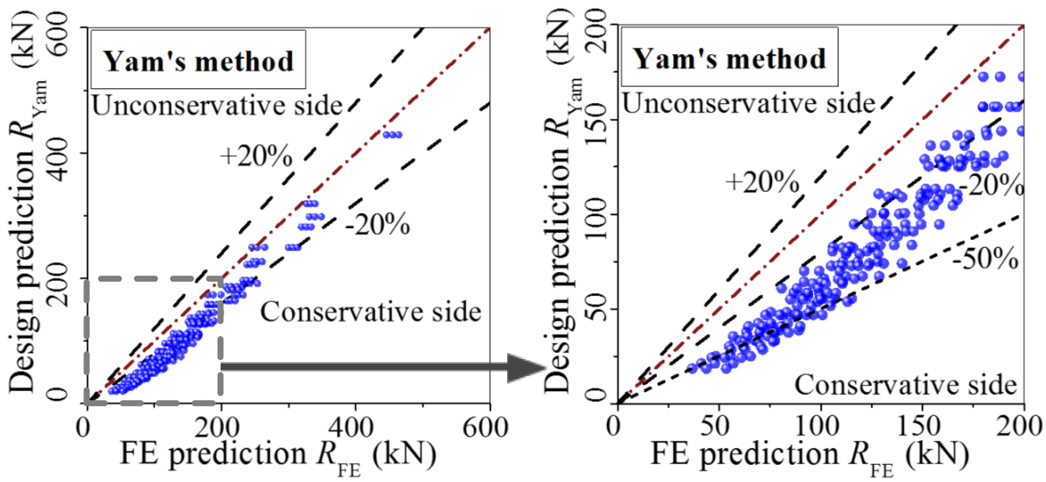

(b)

Fig. 10 Comparison between FE results and design predictions: (a) Cheng’s method and (b) Yam’s method.

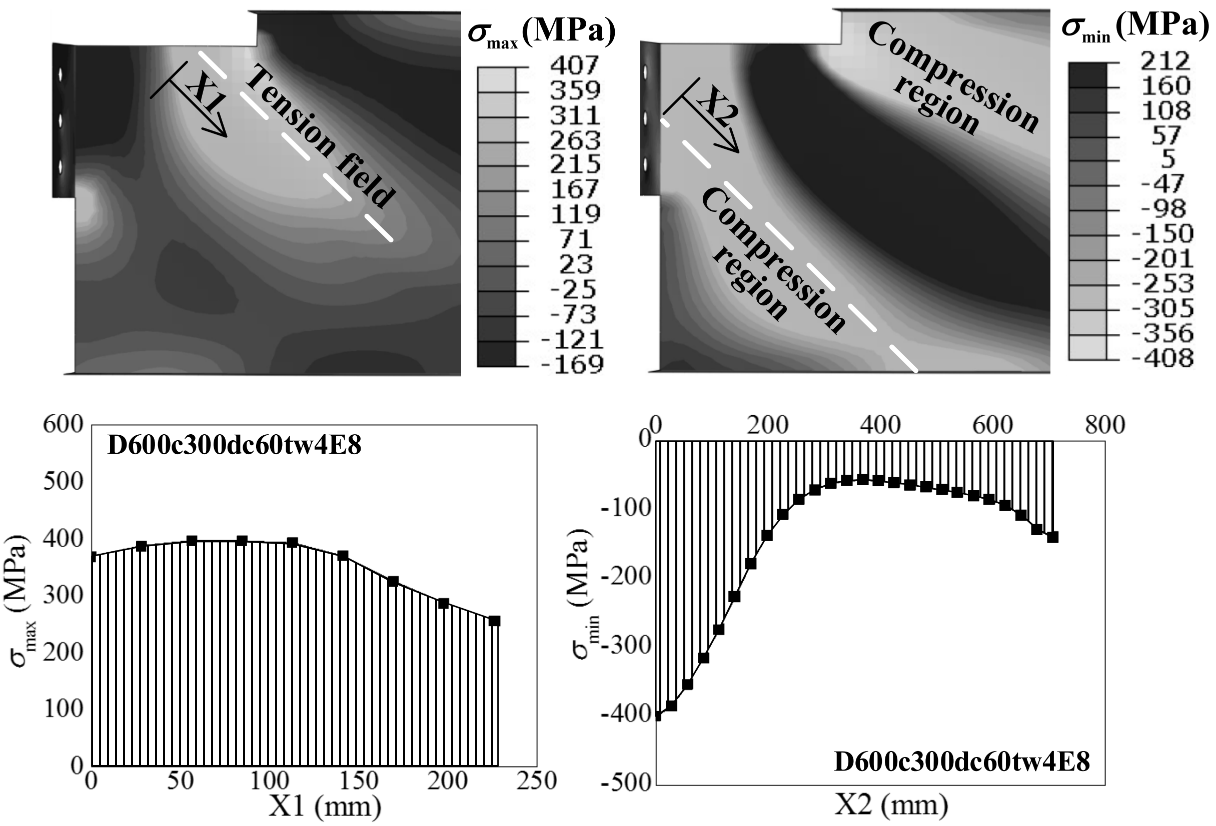

Fig. 11 Stress distribution of a representative SCBSW model in the post-buckling stage.

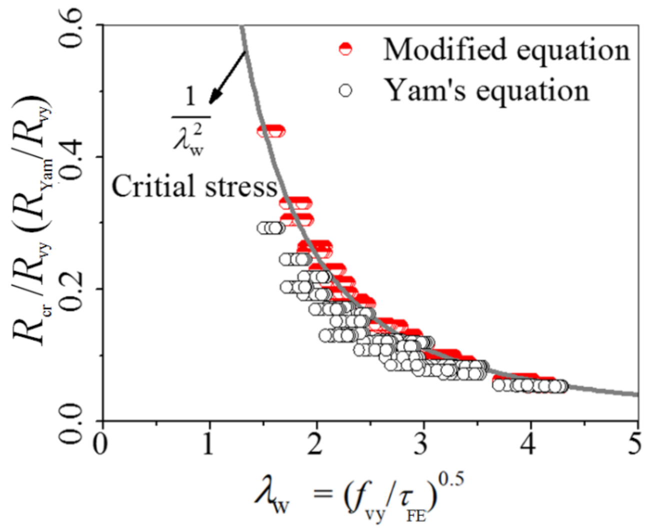

(a)

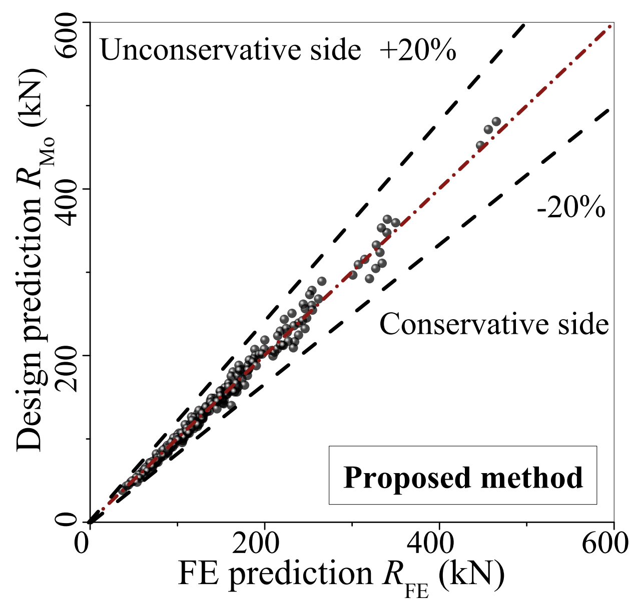

(b)

Fig. 12 Comparison between FE results and design predictions: (a) comparison of elastic buckling strength, and (b) comparison of the ultimate connection strength.

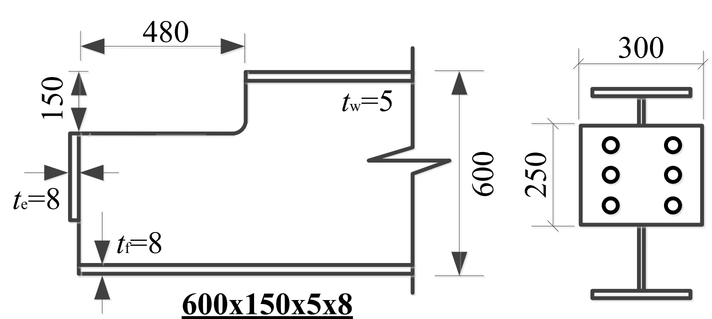

Fig. 13 Geometric dimensions for illustrative design example.

Table 1 Test results, FE predictions and design predictions of specimens from [15].

Specimen code [15]	c/D	d_c/D	D/t_w	R_u (kN)	R_{FE} (kN)	R_{Mo} (kN)	R_u/R_{FE}	R_u/R_{Cheng}	R_u/R_{Yam}	R_u/R_{Mo}
A300dc60	0.5	0.1	102.9	214.0	215.8	203.4	0.99	1.29	1.26	1.08
A300dc120	0.5	0.2	102.9	174.0	167.6	154.6	1.04	1.25	1.38	1.18
A300dc180	0.5	0.3	102.9	139.1	131.0	124.0	1.06	1.23	1.42	1.20
A600dc60	1.0	0.1	102.9	104.9	105.2	94.6	1.00	1.86	1.47	1.15
B375dc75	0.5	0.1	129.1	162.6	162.3	158.8	1.00	1.29	1.21	0.91
B375dc150	0.5	0.2	129.1	143.7	144.7	128.6	0.99	1.36	1.44	1.02
B375dc225	0.5	0.3	129.1	117.2	118.1	107.7	0.99	1.35	1.51	1.02
C300dc60	0.5	0.1	157.1	70.0	70.0	61.2	1.00	1.47	1.55	1.01
C300dc120	0.5	0.2	157.1	60.7	62.3	52.8	0.97	1.53	1.80	1.04
C300dc180	0.5	0.3	157.1	48.8	48.4	46.4	1.01	1.5	1.86	0.98
C600dc60	1.0	0.1	157.1	40.4	40.6	35.6	0.99	2.49	2.12	1.02
						Mean	1.01	1.51	1.55	1.05
						CoV	0.04	0.25	0.18	0.08

Table 2 Parameter spectrum of the numerical study.

Parameter (Unit)	Range	Remarks (Unit: mm)
D (mm)	600, 750, 900	-
c/D	0.5, 0.7, 1.0	c = 300, 375, 420, 450, 525,600, 630, 750, 900
d_c/D	0.1, 0.2, 0.3	d_c = 60, 75, 90, 120, 150, 180, 225, 270
D/t_w	100, 120, 150	t_w = 4.00, 5.00, 6.00, 6.25, 7.50, 9.00
K(10^3kNm/rad)	0.11-0.57	End-plate connection, t_e = 8, 12, 16

Table A1 Information about specimen PB26A [5, 6]

Measured dimensions (Unit:mm)					
D	b_f	t_f	t_w	c	d_c
673.1	152.4	4.6	3.4	332.7	28.7

Material section property (Unit: MPa)			
Yield strength (flange)	Ultimate strength (flange)	Yield strength (web)	Ultimate strength (web)
393	546	410	460

Table A2 Information about basic FE models in the parametric study (Unit:mm)

D	B	t_w	d_c	d_c/D	D/t_w
600	150	4	60	0.1	150
600	150	4	120	0.2	150
600	150	4	180	0.3	150
600	150	5	60	0.1	120
600	150	5	120	0.2	120
600	150	5	180	0.3	120
600	150	6	60	0.1	100
600	150	6	120	0.2	100
600	150	6	180	0.3	100
750	150	5	75	0.1	150
750	150	5	150	0.2	150
750	150	5	225	0.3	150
750	150	6.25	75	0.1	120
750	150	6.25	150	0.2	120
750	150	6.25	225	0.3	120
750	150	7.5	75	0.1	100
750	150	7.5	150	0.2	100
750	150	7.5	225	0.3	100
900	150	6	90	0.1	150
900	150	6	180	0.2	150
900	150	6	270	0.3	150
900	150	7.5	90	0.1	120
900	150	7.5	180	0.2	120
900	150	7.5	270	0.3	120
900	150	9	90	0.1	100
900	150	9	180	0.2	100
900	150	9	270	0.3	100

Conflict of Interest

There is no financial/personal interest or belief that could affect our objectivity. There are no potential conflicts of interest either.